Materials & Design 219 (2022) 110801

Contents lists available at ScienceDirect

Materials & Design

journal homepage: www.elsevier.com/locate/matdes

Immediately implantable extracellular matrix-enriched osteoinductive hydrogel-laden 3D-printed scaffold for promoting vascularized bone regeneration *in vivo*

Jae Seo Lee [a,1], Haram Nah [a,1], Donghyun Lee [b], Sang-Hyun An [b], Wan-Kyu Ko [c], Sang Jin Lee [d], Seung Yeon Lee [e], Kyung Min Park [f], Jung Bok Lee [g], Hyeong-joong Yi [h], Il Keun Kwon [d], Kyu-Sun Choi [h,*], Dong Nyoung Heo [d,i,*]

[a] Department of Dentistry, Graduate School, Kyung Hee University, 26 Kyungheedae-ro, Dongdaemun-gu, Seoul 02447, Republic of Korea
[b] Preclinical Research Center, Daegu-Gyeongbuk Medical Innovation Foundation (DGMIF), Daegu 41061, Republic of Korea
[c] Department of Neurosurgery, CHA University, CHA Bundang Medical Center, Gyeonggi-do 13496, Republic of Korea
[d] Department of Dental Materials, School of Dentistry, Kyung Hee University, 26 Kyungheedae-ro, Dongdaemun-gu, Seoul 02447, Republic of Korea
[e] Department of Biomedical Science and Technology, Graduate School, Kyung Hee University, 26 Kyungheedae-ro, Dongdaemun-gu, Seoul 02447, Republic of Korea
[f] Department of Bioengineering and Nano-bioengineering, Incheon National University, Incheon 22012, Republic of Korea
[g] Department of Biological Science, Sookmyung Women's University, Cheongpa-ro 47-gil 100, Yongsan-gu, Seoul 04310, Republic of Korea
[h] Department of Neurosurgery, College of Medicine, Hanyang University, 222 Wangsimni-ro, Seongdong-gu, Seoul 04763, Republic of Korea
[i] Biofirends Inc., 26 Kyungheedae-ro, Dongdaemun-gu, Seoul 02447, Republic of Korea

HIGHLIGHTS

- The fabricated osteoinductive bioscaffold provided mechanical support and resisted physical stress for bone tissue regeneration.
- The human bone marrow-derived mesenchymal stem cell–derived matrisome promoted osteogenesis.
- Human bone marrow-derived mesenchymal stem cells adhered to the collagen-fibrin matrix, which promoted osteogenic differentiation.
- The polycaprolactone/collagen-fibrin/human bone marrow-derived mesenchymal stem cell–derived matrisome scaffold accelerated a vascularized new bone regeneration *in vivo*.

GRAPHICAL ABSTRACT

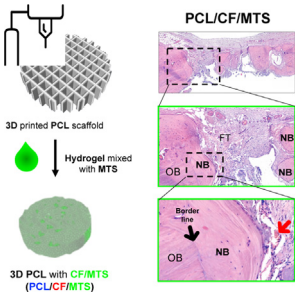

ARTICLE INFO

Article history:
Received 24 March 2022
Revised 27 May 2022
Accepted 28 May 2022
Available online 6 June 2022

Keywords:
Polycaprolactone

ABSTRACT

Reconstruction of patient-specific scaffolds to repair uniquely shaped bone defects remains a major clinical challenge in tissue engineering. Recently, three-dimensional (3D) printed scaffolds have received considerable attention as a promising technology for the rapid generation of custom shapes. However, synthetic polymers commonly used for 3D printing, such as polycaprolactone (PCL), lack the biological capacity to mimic native extracellular matrix functions to support cell growth and differentiation into desired tissues. We described the preparation and characterization of a 3D hybrid model for bone tissue engineering that comprises an extracellular matrix (ECM)-enriched hydrogel embedded in a PCL scaffold. The human bone marrow-derived mesenchymal stem cell–derived matrisome (BMTS) was utilized as a

* Corresponding authors at: Department of Dental Materials, School of Dentistry, Kyung Hee University, 26 Kyungheedae-ro, Dongdaemun-gu, Seoul 02447, Republic of Korea (D.N. Heo). Department of Neurosurgery, College of Medicine, Hanyang University, 222 Wangsimni-ro, Seongdong-gu, Seoul 04763, Republic of Korea (K.S. Choi).
E-mail addresses: vertex-09@hanmail.net (K.-S. Choi), heodaeng@khu.ac.kr (D. Nyoung Heo).
[1] These authors contributed equally to this work.

https://doi.org/10.1016/j.matdes.2022.110801

Biomacromolecules
3D printing
3D hybrid model
Bone tissue engineering

source of ECM-enriched biomacromolecules, and scaffold biocompatibility was evaluated *in vitro* using human bone marrow-derived mesenchymal stem cells (BM-MSCs). The 3D hybrid model exhibited excellent BM-MSC viability and osteogenic activity *in vitro* in both two-dimensional (2D) and 3D cultures. Furthermore, bone remodeling was evaluated by *in vivo* through a rat calvarial defect model; notably, the fabricated 3D hybrid model effectively enhanced vascularized bone regeneration. Therefore, this promising BMTS-based 3D hybrid model might serve as an excellent bone tissue-engineered scaffold for use in orthopedic applications.

1. Introduction

Bone is composed of a hierarchically divided structure. It primarily consists of hydroxyapatite embedded in numerous collagen bundles. Due to combined rigid inorganic and flexible organic components, this arrangement provides a distinctive combination of outstanding mechanical and biological functionalities [1]. Accordingly, bone remodeling is difficult owing to challenges in mimicking the natural bone state during injury or tissue loss. Bone healing is not readily achieved when the damaged region exceeds the critical defect area. This degree of damage requires scaffolds to support new growth and induce tissue regeneration [2].

The integration of three-dimensional (3D) structures and multifunctional components allows the fabrication of engineered components, which due to their proper mechanical properties and interactions with the surrounding natural tissue for damaged bone tissue repair [3]. However, most conventional 3D scaffolds are composed of a non-functional biomaterials. Such systems may not be able to actively interact with the surroundings or adapt to the changes in healing tissue [4]. Therefore, bone tissue-engineered composite scaffolds should be composed of a hard structure and a soft with sophisticated biopolymer for balance. Polycaprolactone (PCL) porous scaffold, a solid fundamental substrate, has been widely used and fabricated using 3D printing technology, as it provides a solid structural framework that contains soft scaffold components [5]. PCL has frequently been used as a 3D printing scaffold due to its substantial mechanical properties and ability to imitate intricate anatomic features with excellent formability [6]. Despite its robust structure as an implant in the human body, PCL is inherently hydrophobic and has relatively poor biocompatibility [7,8]. In addition, PCL must be sintered at a high temperature during 3D fabrication process, which does not allow to incorporate growth factors or living cells [9]. To compensate for these shortcomings, a hydrogel filler is embedded in a 3D scaffold post-fabrication [10]. As a supporting component, various hydrogels have been used due to excellent biocompatibility and a high loading efficiency of stem cells [11]. For example, 3D-printed PCL scaffolds are filled with a natural polymer-based hydrogel composed of collagen and fibrinogen [12]. Collagen accounts for up to 90% of the organic matrix of bone and has a high water content [13]. Its high hydrophilicity offsets the disadvantages of PCL and enhances cell affinity. Subsequently, fibrin, a natural biopolymer derived from fibrinogen during blood coagulation, has been added to the matrix, which provides improved mechanical strength via rapid clotting and assists in tissue repair [14]. Although these scaffolds show significant advantages, collagen and fibrinogen composition are still far from that of the natural bone extracellular matrix (ECM). The BMTS is obtained from the native ECM, which is derived from human bone marrow-derived mesenchymal stem cells (BM-MSCs) and contains over 300 proteins and related cytokines [15]. Thus, ECM-derived biomacromolecules, collectively termed the human bone marrow-derived mesenchymal stem cell–derived "matrisome" (BMTS), loaded hydrogel combined with bioscaffold system is required to directly supply into damaged bone tissue as a differentiation factor [16].

In this study, we fabricated a hybrid soft and hard tissue composite system by incorporating ECM-enriched BMTS within a 3D-printed PCL scaffold as a hybrid 3D model. The porous and rigid 3D-printed PCL scaffold forms a framework for the desired structure. Subsequently, the solid frame is coated with natural polymer-based hydrogels, which are expected to provide biocompatibility and biomolecule loading capacity. Consequently, ECM-enriched BMTS is expected to improve bone regeneration and mimic structures to better match human body conditions. We aimed to physicochemically evaluate the hybrid 3D scaffold and confirm its biocompatibility and osteogenesis *in vitro* and *in vivo*.

2. Experimental section

2.1. Materials

PCL (MW 45,000), fibrinogen, thrombin, and acetic acid were purchased from Sigma-Aldrich (St. Louis, MO, USA). Collagen (atelocollagen) was purchased from Dalim Tissen Co., Ltd. (Seoul, South Korea). HumaTein (BMTS) was purchased from ROKIT Healthcare (Seoul, South Korea). Dulbecco's phosphate buffered saline (DPBS) and trypsin-ethylenediaminetetraacetic acid (EDTA) were purchased from Gibco BRL (Invitrogen, Carlsbad, CA, USA). Cell Counting Kit-8 (CCK-8) was purchased from Dojindo (Kumamoto, Japan).

2.2. Design and fabrication of 3D-printed PCL scaffolds

Briefly, 3D-printed PCL scaffolds were designed using computer-aided design based on our previous study [10]. To supply mechanical hardness, 3D-printed PCL scaffolds were fabricated using a fused deposition modeling 3D printer (Dr. INVIVO; ROCKIT Healthcare).

2.3. Fabrication of collagen-fibrin (CF) hydrogel and CF/BMTS-incorporated PCL scaffolds

The preparation of CF hydrogel is described in our previous study [17]. Briefly, collagen solutions were prepared by mixing acidic collagen solution (50%) with DPBS (10%), distilled water (40%), and 0.2 N sodium hydroxide (10%), and the pH was adjusted to 7.4. Subsequently, fibrin was prepared using thrombin (6 U/mL) and fibrinogen (20 mg/mL in DPBS). The fibrin hydrogel was then mixed with the collagen solution at a 1:1 vol ratio and coated onto the 3D-printed PCL scaffold.

2.4. Rheological properties and morphological analysis of CF and CF/BMTS scaffold

The elastic and viscous moduli were determined using a rotating rheometer (MCR 92; Anton-Paar, Graz, Austria) according to our previous study [18]. All samples were prepared in the form of a disk and measured using a rotating rheometer with a plate-plate geometry with an 8 mm diameter and a 1 mm gap to investigate the frequency-dependent viscoelastic activity. Frequency

sweeps were performed in the range of 0.1–4.0 Hz at a constant strain of 1%. The formulas for calculating $\mathbf{G}'$ and $\mathbf{G}''$ are as follows:

$$\mathbf{G} = \frac{\sigma_0}{\varepsilon_0}\cos\delta, \mathbf{G} = \frac{\sigma_0}{\varepsilon_0}\sin\delta$$

PCL, PCL/CF, and PCL/CF/BMTS morphologies were observed using field emission scanning electron microscopy (FE-SEM; SU8010; Hitachi, Tokyo, Japan) at an acceleration voltage of 5 kV. All freeze-dried samples were taken from cross-sectioned layers across the PCL structure and then sputter-coated with platinum (30 mA) using an MC1000 Ion Sputter Coater (Hitachi, Japan) for 150 s.

2.5. Antibody array analysis

The experimental procedure using the Human L2000 Array is briefly described as follows: the array kit can simultaneously detect 2,000 cytokines, chemokines, adipokines, growth factors, angiogenic factors, proteases, soluble receptors, soluble adhesion molecules, and other proteins. The experiments were conducted in accordance with the manufacturer's guidelines. Antibody array slides (RayBiotech, Norcross, GA, USA) were dried and incubated with a blocking solution for 30 min. Each slide was incubated with 400 μL of the diluted sample for 2 h at room temperature after decanting the blocking buffer. Thereafter, each array slide was washed thrice with 800 μL of wash buffer with shaking. The slides were incubated with biotin-conjugated anti-cytokine antibodies for 2 h at room temperature with gentle shaking. The slides were washed and incubated with Cy3-conjugated streptavidin for 2 h at room temperature. Finally, the slide was washed, rinsed with deionized water, and centrifuged at 1000 rpm for 3 min to remove the water. Signals were detected and visualized by adding a detection mixture and using a chemiluminescence imaging system (Bio-Rad Laboratories, Hercules, CA, USA). Original signal intensities of the proteins were determined using densitometry and standardized using positive controls after correction. The relative protein expression levels were determined by comparing the obtained values to the standardized values.

2.6. Cell culture

Human BM-MSCs (PT-2501; Lonza, Basel, Switzerland) and green fluorescent protein-labeled BM-MSCs (GFP-BM-MSC; HUXMA-01101; Cyagen, Santa Clara, CA, USA) were used at passage six for all cell experiments. Both BM-MSCs and GFP-BM-MSCs were cultured in growth medium (GM), which comprised mesenchymal stem cell basal medium (PT-3238, Lonza) supplemented with fetal bovine serum, L-glutamine, and gentamicin (supplement kit; PT-4105, Lonza). BM-MSCs were incubated in a humidified 5% CO_2 incubator (Heracell VIOS 250i, Thermo Fisher Scientific). Fresh medium was replaced every two days during cell cultivation.

2.7. BM-MSC behaviors in two different dimensions

BM-MSCs were cultured in GM and encapsulated within CF hydrogel at a density of cells/mL. After 1, 4, and 7 days, the samples were washed twice with DPBS and treated with CCK-8 solution according to the manufacturer's instructions. Briefly, the solution was diluted with serum-free GM (without supplementation). After incubation for 2 h, the absorbance was measured using a microplate reader (Bio-Rad Laboratories) at a wavelength of 450 nm.

To visualize cell proliferation in two different dimensions during cultivation, GFP-BM-MSCs were cultured in GM for 7 days. GFP-BM-MSCs were cultured on PCL, PCL/CF, or PCL/CF/BMTS with cells seeded on the scaffold surface or encapsulated in the scaffolds. Growing cells were observed and characterized using the EVOS FL Auto Cell Imaging System (EVOS-M7000; Thermo Fisher Scientific).

2.8. Quantitative real-time polymerase chain reaction (qRT-PCR)

To evaluate osteogenic gene expression of the PCL/CF/BMTS scaffold, BM-MSCs at a density of cells/mL were encapsulated in CF or CF/BMTS hydrogels and cultured using a BM-MSC Osteogenic Differentiation Medium BulletKit (PT-3002; Lonza) for 2 and 4 weeks, respectively. Whole samples were washed with DPBS and treated with TRIzol® reagent (Invitrogen, 15596018) for total RNA isolation. Subsequently, the isolated total RNA was transcribed into cDNA using AccuPower® RT PreMix and Master Mix (Bioneer, Daejeon, Korea). Quantispeed SYBR mix (PhileKorea, Seoul, Korea) and primers were added to the synthesized cDNA for analysis (Table 1). All results were normalized to those for glyceraldehyde-3-phosphate dehydrogenase (GAPDH).

2.9. In vivo implantation of PCL/CF/BMTS-incorporated scaffolds

All animal experiments were performed in compliance with protocols approved by the Institutional Animal Care and Use Committee of Daegu-Gyeongbuk Medical Innovation Foundation (DGMIF, DGMIF-20030404–01). Eleven-week-old male Sprague–Dawley rats (Koatech, Gyeonggi-do, Korea) were divided into four groups: the control (no treatment), PCL, PCL/CF, and PCL/CF/BMTS groups. Animal care and treatment were conducted in accordance with the guidelines established by the Institutional Animal Care and Use Committee (IACUC; DGMIF-20030404–01). A midline incision was made over the calvarium, and a full-thickness flap was elevated. A critical size calvarial defect (5 mm) was created using a trephine bur under sterile saline irrigation. After the lesion was formed, the respective scaffold compositions were applied to fill the area. The incisions were sutured in layers with 5–0 chromic gut and 4–0 silk sutures. All animals received a single intramuscular injection of cefazolin (30 mg/kg) 2 d after the surgery. The animals were sacrificed 4 and 8 weeks after the surgery.

2.10. Microscopic and histological evaluations

At 4 or 8 weeks post-implantation, the rats in each group were sacrificed, and their surgical sites were harvested and fixed in 10% neutral buffered formalin. These sections were imaged by micro-computed tomography (μCT) using a SkyScan 1172 (Bruker, Billerica, MA, USA) scanner in accordance with our previous study [18]. According to μCT, the degree of bone was quantified using the average gray value and standard deviation of the region of interest. For μCT analysis, new bone volume (mm^3), percent bone volume ratio (bone volume/tissue volume, %), and bone mineral density (mg/cc) were quantified.

After sacrifice, calvarial samples were fixed in neutral formalin and decalcified using EDTA. Each sample was embedded in paraffin and sectioned. The sections were stained with hematoxylin and eosin (H&E) and Masson's trichrome for microscopic histological evaluation.

2.11. Statistical analysis

All data are presented as mean ± standard deviation. Statistical analysis of the significance of differences between groups was performed by two-way analysis with Bonferroni's multiple comparison test using GraphPad Prism version 7 (GraphPad Software, San Diego, CA, USA). Statistical significance was set at $^{*}p < 0.05$, $^{**}p < 0.01$, and $^{***}p < 0.001$.

Table 1
Primer sequences of osteogenic differentiation related for real-time polymerase chain reaction (qRT-PCR).

Gene	Forward 5′–3′	Reverse 5′–3′
COL1	ATCACCTGCGTACAGAACGG	CGTCATCGCACAACACCTTG
OCN	CCAGGCGCTACCTGTATCAA	TCAGCCAACTCGTCACAGTC
OPN	CTGAACGCGCCTTCTGATTG	ATCTGGACTGCTTGTGGCTG
BSP	GGGCACCTCGAAGACAACAA	GCCCGTGTATTCGTACTCCC
BMP2	CGAAATTCCCCGTGACCAGA	GAATCCATGGTTGGCGTGTC
GAPDH	ATTCCATGGCACCGTCAAGG	TGGACTCCACGACGTACTCA

3. Results and discussion

3.1. Characterization of PCL, PCL/CF, and PCL/CF/BMTS

A schematic representation of the fabrication process of 3D-printed PCL scaffolds filled with CF hydrogel and BMTS is shown in Fig. 1A. First, 3D-printed PCL scaffolds were used as mechanical supports for the composite scaffolds. Furthermore, the PCL scaffold provides an external frame and an internal porous structure that corresponds with bone tissue structure. However, PCL has a low cell affinity and cannot be loaded with cells or biomolecules due to the high-temperature sintering process [19]. Additionally, natural bone is complex and contains both hard and soft tissues [20]. Hence, we used CF hydrogel with a natural-based polymer to fill the frame and better mimic the human bone. In summary, the PCL scaffold was fabricated using an extrusion 3D printing system to maintain the frame of the entire scaffold. Subsequently, insufficient biocompatibility of PCL was corrected by filling the porous structure of the scaffold with CF hydrogel and BMTS to create a composite scaffold.

Dynamic rheological properties were measured to confirm the rheological differences between CF hydrogel and the PCL/CF and PCL/CF/BMTS scaffolds (Fig. 1B). The scaffolds were gelled to equilibrium and studied at room temperature. The CF hydrogel showed rheological properties at < 500 Pa, which correspond to those of a soft hydrogel [21]. Furthermore, the PCL/CF scaffold showed increased G and G″ values relative to those of the CF hydrogel, representing the stiffness imparted by the PCL scaffold reinforcing the CF hydrogel. However, integrating BMTS into the PCL/CF scaffold did not cause any differences in physical properties; the stiffness was unaffected owing to the small molecular size of BMTS [22]. As shown in Fig. 1C, similar cross-section SEM images of the inner microporous structure of the PCL/CF and PCL/CF/BMTS scaffolds supported this result. Regarding the PCL group, the scaffold consisted only of the support frame without inner components. In contrast, in the PCL/CF and PCL/CF/BMTS groups, the gels were embedded within the entire PCL structure, forming an integrated body. Imaging at a higher magnification indicated that the pores inside the structures were well interconnected, which allows for the transportation of water and nutrients [23]. Additionally, CF can encapsulate other biomolecules and cells. We observed no differences in the inner structures of the PCL/CF/BMTS scaffold compared to those of the PCL/CF scaffold, indicating that the pore size of the PCL structure was not affected by BMTS owing to its small molecular size.

Also, proteomic analysis was performed to determine the effect of BMTS on cellular behavior. BMTS can be extracted from various tissues, such as bone, fat, and skin. Despite different protein origins, a common protein appears, and the number of matrix proteins exists within the same range. However, relatively high collagen levels are expressed in BM-MSCs compared to those in other tissues. Notably, the fibrillar collagen family is involved in tissue stiffness or strength, directly affecting mechanical strength. It also upregulates genes involved in cell adhesion at an early stage and is more sensitive to ECM signals [10]. Thus, BM-MSC–based BMTS was selected to construct new bone in this study. BMTS proteins are organized into two categories: core and BMTS-associated proteins (Fig. 2A). Core proteins are mainly composed of collagen and glycoproteins, which account for approximately 75% of the total mass. These proteins perform various functions that reinforce cell adhesion and provide signaling via integrin binding [24–26]. Collagens are important as they provide the structural support of the ECM (Fig. 2B). Several collagens that contribute to the molecular structure and mechanical properties of many tissues due to their high energy storage capacity and minimal elasticity have been identified [27]. In particular, collagen type IV is the most abundant collagen and enhances beaded filament formation [28]. Moreover, fibrillar collagen accounts for the second largest proportion and is abundant in bones as it resists stretching [29]. Furthermore, glycoproteins (fibulin 4 and fibrinogen γ) are highly stable due to their multidomain structures and bind to adhesion molecules that mediate ECM protein assembly [27,30]. The rest of the ECM comprises secreted factors and BMTS-associated proteins. Numerous BMTS-associated proteins include those that regulate the ECM; for example, HtrA serine peptidase 1, matrix metallopeptidase 2, and lysyl oxidase-like 1/2 control the fine balance between stability and remodeling and form cross-links between fibrils, resulting in structural mechanical strength. These secreted factors are also responsible for regulating stem cell homeostasis through various cellular processes, such as cell proliferation and differentiation control [16]. Further information regarding the core matrix and matrix-associated proteins is provided in Table 2. Our results suggested that BMTS provided a favorable environment for cell proliferation and differentiation in response to the respective secreted factors.

3.2. Comparison of cell viability and osteogenic gene expression in PCL/CF/BMTS scaffolds between different cell culture dimensions in vitro

To confirm the biocompatibility of the developed hybrid 3D scaffolds, we incubated the cells in both two (cells seeded on the surface) and three (cell encapsulation) dimensions relative to the scaffold. Considering both dimensions for the evaluation of implantable biomaterials used in tissue engineering is biologically important, as scaffolds are implanted in the 3D ECM environment in the body, which is in contact with the scaffold surface [31,32]. We assayed 2D cellular behavior to evaluate cell-surface interactions (Fig. 3). BM-MSCs were seeded on the PCL, PCL/CF, or PCL/CF/BMTS scaffold surfaces. On the first day of measurements, the PCL/CF and PCL/CF/BMTS groups showed significantly higher proliferation rates than did the PCL group, with 135% and 159% increases, respectively (Fig. 3A). This upregulation of cell proliferation was also observed on days 4 and 7. On day 7, the proliferation rates of the PCL, PCL/CF, and PCL/CF/BMTS groups were 141%, 259%, and 323%, respectively, compared to that of the PCL group on day 1.

The low rate of increase in cell proliferation on PCL is due to the smaller surface area of the PCL scaffold to which cells can attach than that of the CF hydrogel-embedded PCL. The 3D-printed PCL by itself provided a relatively hydrophobic surface, the porosity of which is insufficient for good cell affinity to induce cell attachment [33,34]. Additionally, the open PCL scaffold structure (in the absence of filling hydrogel) provides a large space inside the support, which limits its ability to hold cell clusters for tissue regeneration. Gupta et al. previously described that the 3D-printed PCL surface treated with NaOH etching could provide suitable roughness and porosity for enhanced cellular attachment [35]. For our purposes, we decided to improve BM-MSC adhesion and proliferation by employing a hydrogel that mimics the natural ECM structure in which cells survive, rather than chemically modifying the PCL surface to overcome its limitations. Moreover, PCL/

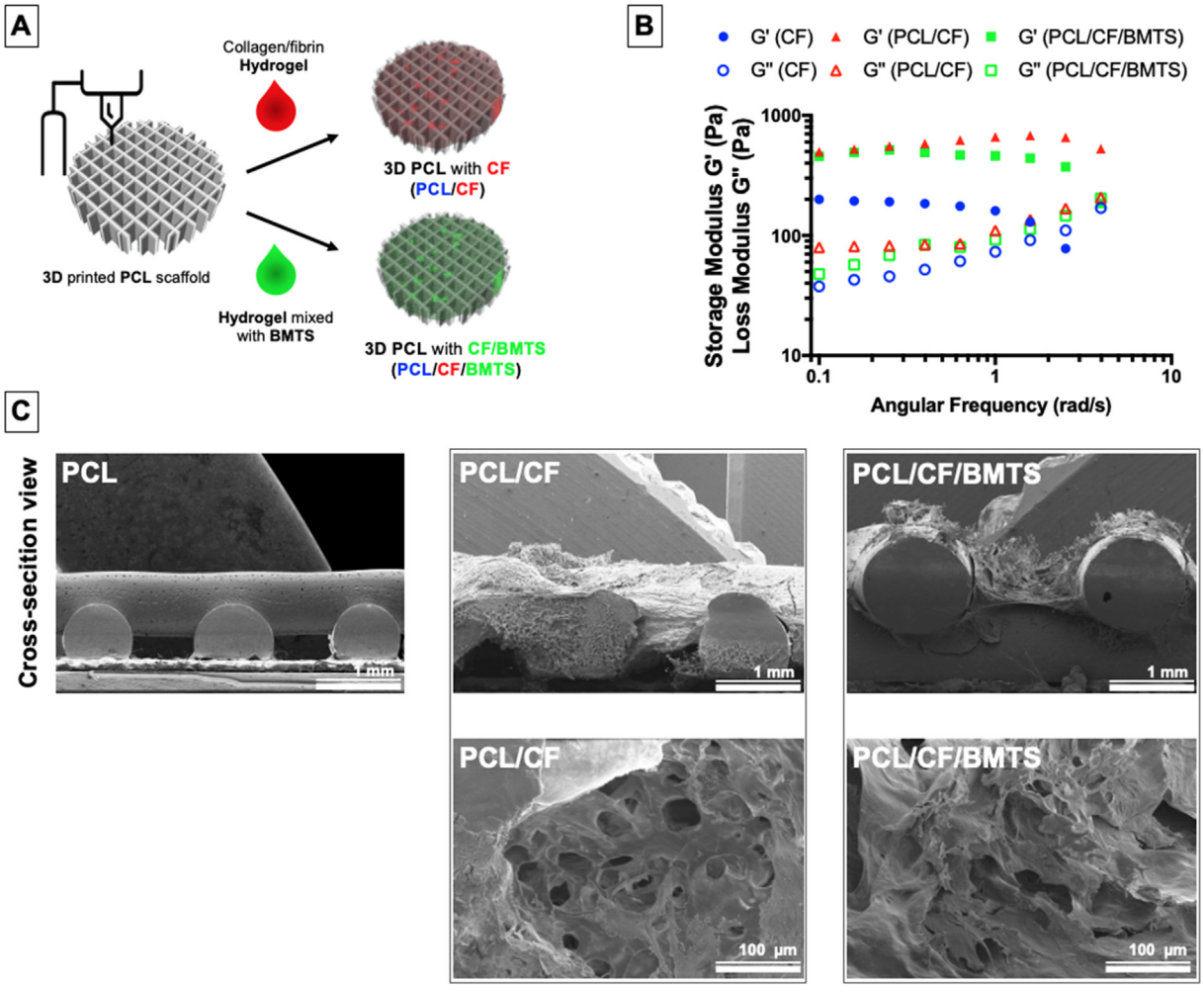

Fig. 1. Illustration and characterization of fabricated 3D hybrid scaffolds: (A) Schematic illustration of 3D-printed polycaprolactone (PCL) scaffolds filled with collagen/fibrin (CF) hydrogel and the CF/human bone marrow-derived mesenchymal stem cell–derived matrisome (CF/BMTS); (B) rheological properties; and (C) cross-section views of the PCL, PCL/CF, and PCL/CF/BMTS scaffolds obtained using field emission scanning electron microscopy (FE-SEM). Scale bars, 1 mm and 100 μm.

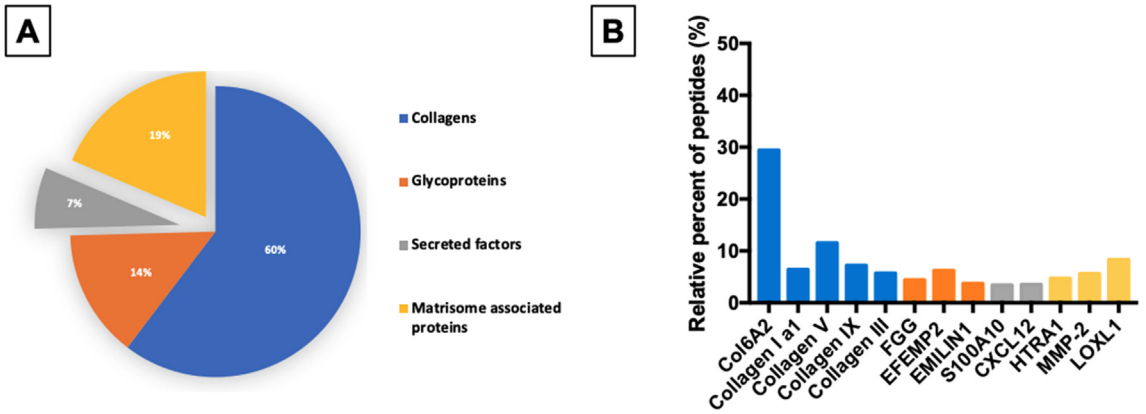

Fig. 2. Proteomic analysis: (A) Pie chart of protein distribution in the human bone marrow-derived mesenchymal stem cell (BM-MSC)-derived matrisome (BMTS). (B) Distribution of quantified proteins. COL6A2, collagen type VI alpha 2 chain; FGG, fibrinogen gamma chain; EFEMP2, EGF containing fibulin extracellular matrix protein 2; EMILIN1, elastin microfibril interfacer 1; S100A10, S100 calcium binding protein A10; CXCL12, C-X-C motif chemokine ligand 12.

CF and PCL/CF/BMTS cells showed large differences in the degree of proliferation. PCL/CF cells had a proliferation rate of 27% between days 1 and 4, whereas PCL/CF/BMTS cells had a proliferation rate of 71% over the same time period. The cell growth rates in the PCL/CF and PCL/CF/BMTS groups increased to 77% and 93%, respectively, between days 4 and 7. BM-MSCs displayed good adhesion and proliferation in all groups; however, the proliferation was particularly high in the PCL/CF/BMTS group (Fig. 3). These results were closely related to the characteristics of the scaffold surrounding the BM-MSCs. The surface area spatially increased via the surrounding

Table 2
Core matrix and matrix-associated proteins expressed by human bone marrow-derived mesenchymal stem cells (BM-MSC)-derived matrisome (BMTS).

Collagens		
	Gene Symbol	***Protein***
Fibril forming	COL1A1	Collagen I α1
	COL3A1	Collagen III α1
	COL5	Collagen V
Network forming	COL4	Collagen IV
Beaded filament forming	COL6	Collagen VI
Glycoproteins		
	Gene Symbol	***Protein***
Major known	EFEMP2	Fibulin 4
	EMILIN1	Emilin 1
Vascular ECM proteins	FGG	Fibrinogen γ
Matrisome associated proteins		
	Gene Symbol	***Protein***
Regulators Proteases	HTRA1	HtrA serin peptidase 1
	MMP2	Matrix metallopeptidase 2
Crosslinkers	LOXL1/2	Lysyl oxidase-like 1/2
Secreted factors		
	Gene Symbol	***Protein***
	S100A10	S100 calcium binding protein A10
	CXCL12	Chemoxin C-X-C motif ligand 12

CF hydrogel, thus increasing the space for cell proliferation. BMTS-associated proteins regulated the ECM, which yielded a proper mechanically strong structure by forming cross-links between the fibrils. Furthermore, BM-MSCs maintained their spindle-like morphologies on the PCL/CF and PCL/CF/BMTS scaffolds. As a result of 2D culture on the scaffolds, the PCL/CF/BMTS group had a significantly higher cell proliferation. These results indicated that cell proliferation increased upon loading BMTS.

Additionally, we focused on the cell encapsulation strategy in the 3D culture. As mentioned above, because the 2D cell culture does not sufficiently mimic the native ECM, we used CF hydrogels as an artificial 3D ECM matrix to provide a native environment for BM-MSCs [31,32,36]. In this experiment, we compared the PCL/CF and PCL/CF/BMTS groups, as PCL alone could not be loaded with cells. As shown in Fig. 4A, the BMTS-treated group had an approximately 22% higher proliferation than the PCL/CF group did from day 1 of cell loading. This pattern continued until day 7, the end of the experiment. On day 7, the growth rate was increased by 76% and 140% in the PCL/CF and PCL/CF/BMTS groups, respectively, compared to that in the PCL/CF group on day 1. Daily variations in the growth rates were the same as those observed in the 2D culture. The PCL/CF group showed a growth rate of 29% from days 1 to 4, whereas the PCL/CF/BMTS group showed a higher growth rate of 59%. Moreover, the growth rates from days 4 to 7 were 50% and 59% for the PCL/CF and PCL/CF/BMTS groups, respectively. This demonstrated that the PCL/CF/BMTS group had a higher growth rate. Interestingly, the increase in proliferation rate was more pronounced in the fluorescence images on day 7 (Fig. 4B); the BMTS-incorporated group demonstrated an BM-MSC-specific fibroblast–like morphology that significantly affects the degree of cellular adhesion [37]. This phenomenon may be involved in glycoproteins, including fibulin-4 and fibrinogen γ, which are associated with adhesion. This indicated that our BMTS-incorporated hydrogel provided a favorable environment for BM-MSC adherence; therefore, our PCL/CF/BMTS scaffolds could have sufficient potential to promote BM-MSC differentiation into mature osteoblasts. Noteworthy, secreted factors in the BMTS might regulate cellular processes. The environmental conditions for cell survival and differentiation are highly important and rely not only on the dynamic mechanical load but also on the mechanical properties of the ECM [38]. Additionally, initial cell attachment is important for tissue regeneration, as both the surface characteristics and biochemical properties of scaffolds can affect cell attachment [39]. The stiffness and porosity characteristics of PCL/CF and PCL/CF/BMTS (Fig. 1B, C) allowed good cell affinity and BM-MSC differentiation. In addition, these *in vitro* results were related to the corresponding proteomic analysis results (Fig. 2 and Table 2). The main components of BMTS, collagen, and glycoprotein play critical roles in mammalian cellular adhesion and binding with the ECM, which directly affected the results of 2D and 3D culture experiments.

Prior to implanting the PCL/CF/BMTS scaffold in a rat calvarial model, we performed an qRT-PCR analysis to confirmed *in vitro* osteogenic ability (Fig. 5). BM-MSCs were well-encapsulated in

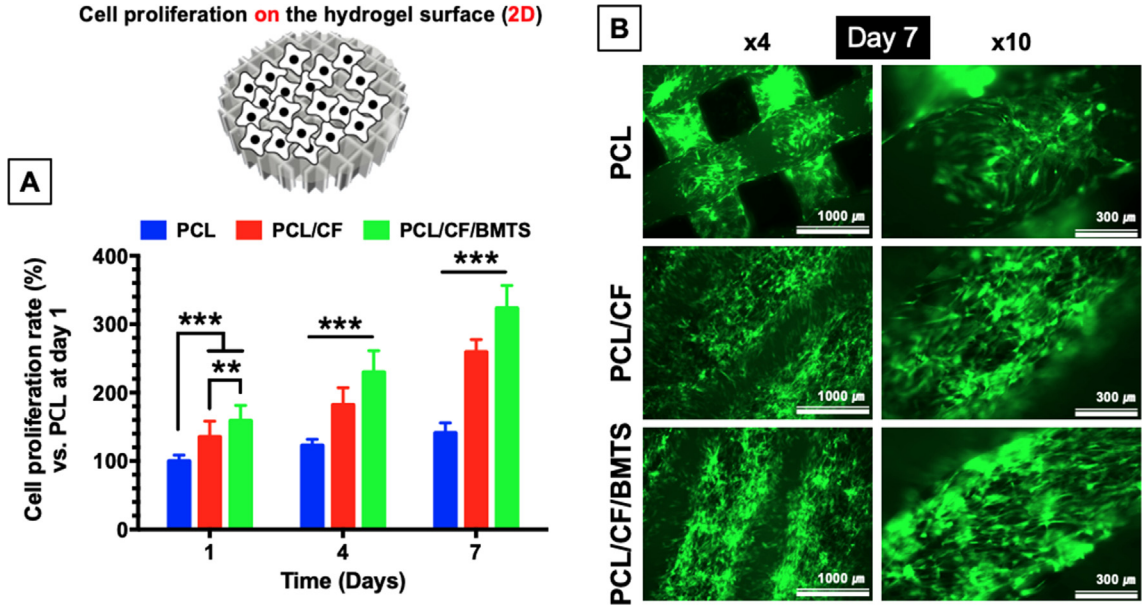

Fig. 3. Evaluation of a two-dimensional (2D) model: (A) proliferation rate and (B) fluorescence images of green fluorescent protein-labeled human bone marrow-derived mesenchymal stem cells (GFP-BM-MSCs) cultured on the surface of polycaprolactone (PCL), PCL with collagen/fibrin (CF, PCL/CF), or PCL with CF/human bone marrow-derived mesenchymal stem cell–derived matrisome (BMTS, PCL/CF/BMTS) scaffolds (n = 6). Scale bars, 1,000 and 300 μm. $^{**}p < 0.01$, and $^{***}p < 0.001$. (For interpretation of the references to colour in this figure legend, the reader is referred to the web version of this article.)

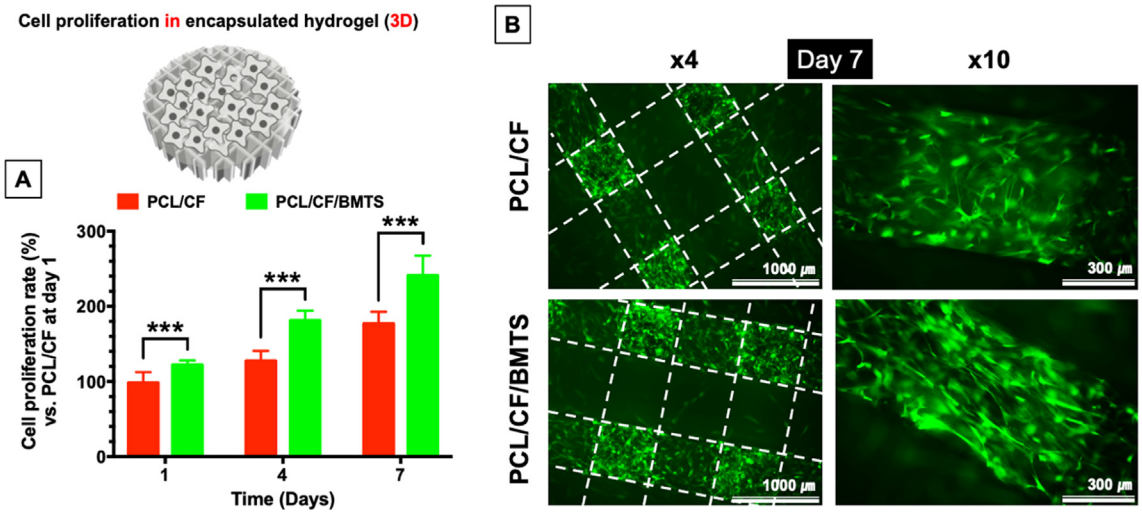

Fig. 4. Evaluation of a three-dimensional (3D) model: (A) proliferation rate and (B) fluorescence images of green fluorescent protein human-labeled bone marrow-derived mesenchymal stem cells (GFP-BM-MSCs) encapsulated in the polycaprolactone (PCL)/collagen-fibrin (CF) or PCL/CF/human bone marrow-derived mesenchymal stem cell–derived matrisome (BMTS) scaffolds (n = 6). Scale bars, 1,000 and 300 μm. ***p < 0.001. (For interpretation of the references to colour in this figure legend, the reader is referred to the web version of this article.)

PCL/CF/BMTS at 2 and 4 weeks after cultivation. Subsequently, we explored whether PCL/CF/BMTS could induce the osteogenic differentiation of BM-MSCs. Notably, qRT-PCR revealed higher expression levels of osteogenic markers such as collagen type 1 (COL1), osteocalcin (OCN), osteopontin (OPN), bone sialoprotein (BSP), and bone morphogenetic protein 2 (BMP2) [18,40,41]. The expression of these time-dependent osteogenic gene markers—particularly BSP expression at 4 weeks after cultivation—was markedly high (Fig. 5C). COL1 is the main component of the ECM of osteoblasts, and BSP levels are the highest among the non-collagenous proteins [42]. Importantly, higher BSP expression levels in the PCL/CF/BMTS group compared to those in the PCL/CF group indicated the osteogenic differentiation of BM-MSCs in the CF hydrogel upon BMTS loading. These results strongly suggested that the main components of BMTS triggered BM-MSC adhesion to the CF matrix and provided sufficient conditions for proliferation and osteogenic differentiation.

3.3. In vivo characterization of new bone tissue formation after PCL/CF/BMTS scaffold implantation in a rat calvarial defect model

To evaluate the bone-remodeling effects of PCL/CF/BMTS, we implanted the scaffolds in calvarial defect-containing rats (Fig. S1), which were sacrificed at 4 and 8 weeks post-implantation. As shown in μCT images, a small amount of bone formation was observed in the PCL group, whereas prominent bone formation was observed around the lesion in the CF and CF/BMTS groups (Fig. 6A). We quantified the amount of new bone using BV (mm^3), BV/TV (%), and BMD (mg/cc; Fig. 6B, C, and D). None of the three groups showed statistically significant differences during the 4-week BV, BV/TV, and BMD evaluation. However, the PCL/CF/BMTS group exhibited the highest rate of new bone formation. Prominent regenerative effects in the PCL/CF/BMTS group were observed after 8 weeks. The BV yield in the PCL/CF/BMTS group was 14.82 ± 0.99 mm^3, which was significantly higher than that in the PCL group (10.78 ± 1.6 mm^3). The results of the BV/TV derived from μCT images indicated a similar trend in BV values; particularly, the PCL/CF/BMTS group (7.55 ± 1.12%) showed more bone growth than the PCL (7.55 ± 1.12%) and PCL/CF (8.86 ± 0.89%) groups did (Fig. 6C). Furthermore, the BMD values at the implantation site of the PCL, PCL/CF, and PCL/CF/BMTS groups were 56.8 ± 8.96, 76.53 ± 2.67, and 85.49 ± 9.85 mg/cc, respectively. This indicated a significantly improved regeneration of the PCL/CF/BMTS group compared to that of the PCL group (Fig. 6D).

Furthermore, we performed H&E staining to histologically evaluate new bone formation in the host tissues (Fig. 7A). In the PCL group, the implanted defect site was filled with a small amount of bone and fibrous tissue. However, the PCL/CF and PCL/CF/BMTS groups showed better new bone formation in direct contact with the host tissue, which was surrounded by fibrous connective tissue. New bone formation appeared as a few bony islands formed in the middle of the fibrous tissues in the PCL/CF/BMTS group [43]. The implanted scaffolds integrated with the newly formed bone and bone matrix and showed excellent osseointegration. Interestingly, new vasculature containing red blood cells appeared with the new bone in the PCL/CF and PCL/CF/BMTS groups (red arrows). In contrast, the PCL group only showed connective tissue in the border area. We hypothesized that the integration of osteoinductive hydrogel induced vasculature and bone formation [44]. Currently, in the bone tissue engineering field, vasculature formation is being considered highly important for healthy new bone formation [45,46]. The healing process, which is divided into several steps, occurs in response to bone damage. First, damaged blood vessels form a hematoma around the defect site, forming a soft callus. Thereafter, the blood vessels grow into the center of the scaffold, keeping the bone alive. New blood vessels are then formed on the outside and inside of the callus and are mineralized into hydroxyapatite to form a hard callus. Eventually, blood is supplied via new vessels, and long-term vascularization and nomotopic rhythm are achieved. Taken together, our results suggested that vascularized bone recruited MSCs to provide a microenvironment for bone growth and reconstruction [47].

We also performed Masson's trichrome staining to evaluate and visualize new bone formation in a rat calvarial defect model (Fig. 7B). The PCL scaffold alone had low biodegradability in the defect area and low compatibility with the host tissue at the implant site. However, the CF and CF/BMTS composite groups exhibited better new bone formation and fibrous tissue surrounding the PCL scaffold. Particularly, specific new bone formation area was larger in the PCL/CF group, but dense fibrous tissues around the new bone formation area were wider in the PCL/CF/BMTS group, which was consistent with the proteomic data (Fig. 2 and

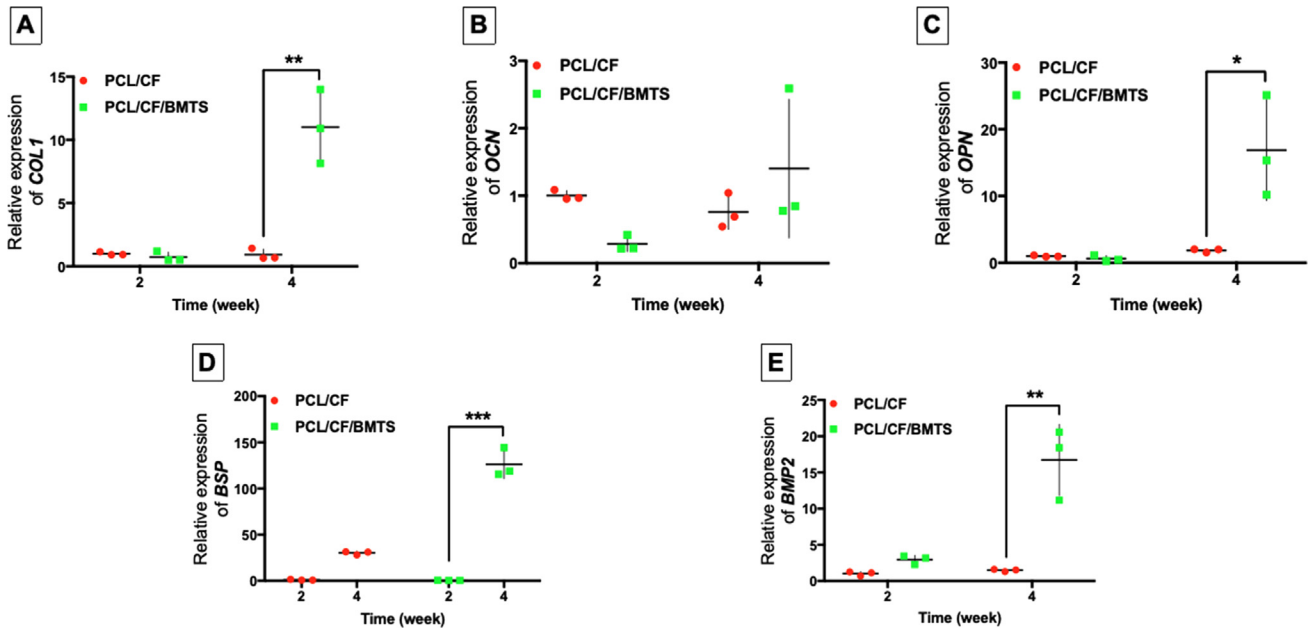

Fig. 5. Evaluation of osteogenic gene expression: (A) collagen type 1 (COL1), (B) osteocalcin (OCN), (C) osteopontin (OPN), (D) bone sialoprotein (BSP), and (E) bone morphogenetic protein 2 (BMP2) (n = 6). *p < 0.05, **p < 0.01, and ***p < 0.001.

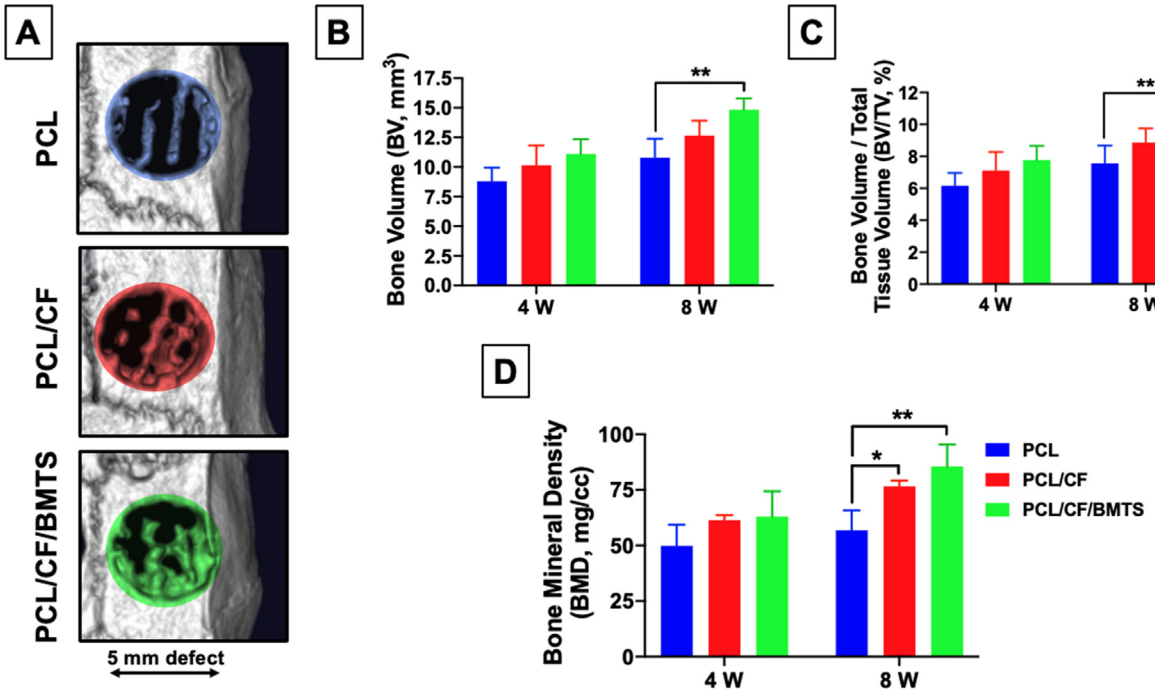

Fig. 6. Bone regeneration in critical-sized calvarial defects: (A) μCT images of calvarial defects implanted with the polycaprolactone (PCL)/collagen/fibrin (CF) or PCL/CF/human bone marrow-derived mesenchymal stem cell–derived matrisome (BMTS) scaffolds. (B) Bone volume (BV), (C) bone volume per total tissue volume (BV/TV), and (D) relative bone mineral density (BMD) obtained from the quantitative analysis of μCT images. *p < 0.05 and **p < 0.01.

Table 1). BMTS contains collagen-like molecules, and collagen is a major component of the native ECM. These results indicated that the PCL/CF/BMTS group formed more new fibrous tissue than the other groups did. In addition, new bony areas in the middle of the fibrous tissues were observed in the PCL/CF/BMTS group. However, the durations of our *in vivo* experiments were relatively short, and longer observations (e.g., 16 weeks or more) will likely provide more conclusive data [48]. Nevertheless, PCL/CF/BMTS allowed for the formation of dense fibrous tissue around the implanted scaffold, leading to more new bone formation. These results demonstrated that the BMTS composite bio-scaffold provided a favorable ECM environment for the formation of more bone tissue, which is also supported by newly generated vasculature visualized using Masson's trichrome staining (red arrows). Therefore, our hybrid 3D scaffold system might not only promote bone formation but also use micro-vessels from the surrounding tissues to remodel vascularized bone tissue. However, further *in vitro* and *in vivo* experiments are required to elucidate the mechanism of vascula-

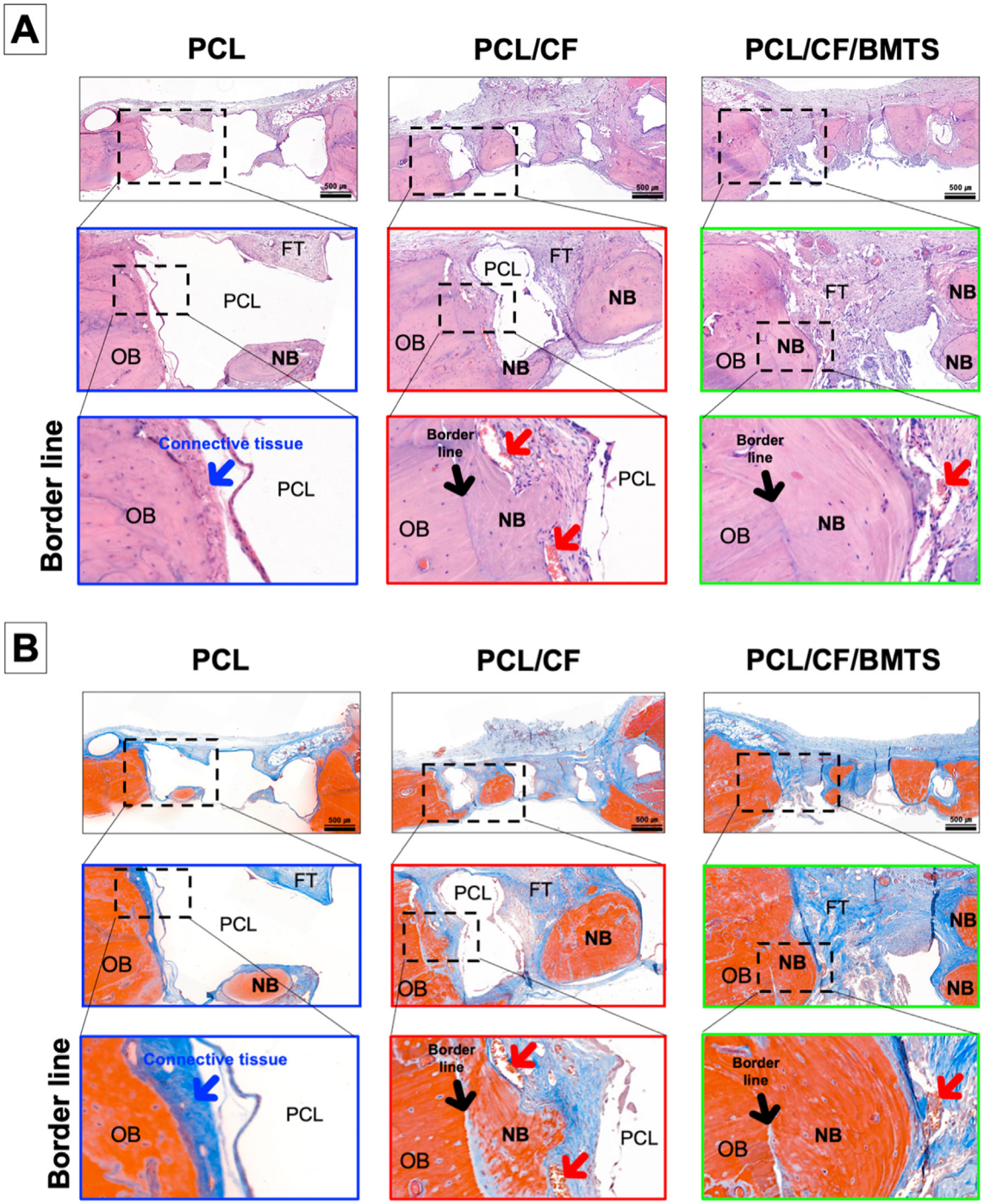

Fig. 7. Histological evaluation of bone regeneration at 8 weeks post-implantation: (A) hematoxylin and eosin (H&E) and (B) Masson's trichrome staining images of the cross-sections of polycaprolactone (PCL)/collagen/fibrin (CF) and the PCL/CF/bone marrow-derived mesenchymal stem cell–derived matrisome (BMTS). Scale bars, 500 μm. Blue, black, and red arrows indicate connective tissue, border line, and red blood cells in vasculature, respectively. PCL, PCL scaffold; OB, old bone; NB, new bone; FT, fibrous tissue; MT, muscle tissue. (For interpretation of the references to colour in this figure legend, the reader is referred to the web version of this article.)

ture formation and its relationship with CF and the BMTS. Nevertheless, the μCT and histology results correlated with the *in vitro* results, which indicated that the BMTS-incorporated bio-scaffold accelerated bone regeneration.

4. Conclusion

In this study, we fabricated a composite scaffold consisting of a 3D-printed PCL filled with the BMTS and CF hydrogel, which enhanced both cellular behavior and bone healing at defect sites by delivering bone tissue-targeting biomacromolecules necessary for regeneration. The 3D-printed PCL scaffold provided mechanical support and resisted physical stress in the bone tissue. Notably, the BMTS induced osteogenic functionality and did not interfere with the original mechanical properties of the scaffold, even after its incorporation into CF hydrogel. Furthermore, the BMTS-incorporated scaffold enhanced BM-MSC proliferation in 2D and 3D cultures and induced the upregulation of osteogenic gene markers. Consequently, the composite scaffold enhanced osteoin-

duction and tissue repair in a critical size defect rat calvarial model. Our study indicated that the BMTS-incorporated 3D-printed scaffold enhanced bone growth and that it might be promising for tissue engineering applications.

Declaration of Competing Interest

The authors declare that they have no known competing financial interests or personal relationships that could have appeared to influence the work reported in this paper.

Acknowledgement

This work was supported by a National Research Foundation of Korea (NRF) grant funded by the Korean government (MSIT) (NRF-2019M3E5D1A01069356, NRF-2020R1C1C1007129).

Appendix A. Supplementary material

Supplementary data to this article can be found online at https://doi.org/10.1016/j.matdes.2022.110801.

References

[1] X. Wang, J. Fang, W. Zhu, C. Zhong, D. Ye, M. Zhu, X. Lu, Y. Zhao, F. Ren, Bioinspired highly anisotropic, ultrastrong and stiff, and osteoconductive mineralized wood hydrogel composites for bone repair, Adv. Funct. Mater. 31 (20) (2021) 2010068.
[2] S. Romanazzo, T.G. Molley, S. Nemec, K. Lin, R. Sheikh, J.J. Gooding, B. Wan, Q. Li, K.A. Kilian, I. Roohani, Synthetic bone-like structures through omnidirectional ceramic bioprinting in cell suspensions, Adv. Funct. Mater. 31 (13) (2021) 2008216.
[3] M. Zhang, R. Lin, X. Wang, J. Xue, C. Deng, C. Feng, H. Zhuang, J. Ma, C. Qin, L.i. Wan, J. Chang, C. Wu, 3D printing of Haversian bone–mimicking scaffolds for multicellular delivery in bone regeneration, Sci. Adv. 6 (12) (2020).
[4] F. Liu, H. Mishbak, P. Bartolo, Hybrid polycaprolactone/hydrogel scaffold fabrication and in-process plasma treatment using PABS, Int. J. Bioprinting 5 (1) (2019).
[5] S.J. Lee, D. Lee, T.R. Yoon, H.K. Kim, H.H. Jo, J.S. Park, J.H. Lee, W.D. Kim, I.K. Kwon, S.A. Park, Surface modification of 3D-printed porous scaffolds via mussel-inspired polydopamine and effective immobilization of rhBMP-2 to promote osteogenic differentiation for bone tissue engineering, Acta Biomater. 40 (2016) 182–191.
[6] J. Park, S.J. Lee, H.H. Jo, J.H. Lee, W.D. Kim, J.Y. Lee, A. Su, Fabrication and characterization of 3D-printed bone-like β-tricalcium phosphate/polycaprolactone scaffolds for dental tissue engineering, J. Ind. Eng. Chem. 46 (2017) 175–181.
[7] Y. She, Z. Fan, L. Wang, Y. Li, W. Sun, H. Tang, L. Zhang, L. Wu, H. Zheng, C. Chen, 3D Printed Biomimetic PCL Scaffold as framework interspersed with collagen for long segment tracheal replacement, Front. Cell Dev. Biol. 9 (2021) 33.
[8] S.J. Lee, H.-J. Kim, M. Heo, H.-R. Lee, E.-J. Choi, H. Kim, D. Lee, R.L. Reis, S.H. Do, I. K. Kwon, In vitro and in vivo assessments of an optimal polyblend composition of polycaprolactone/gelatin nanofibrous scaffolds for Achilles tendon tissue engineering, J. Ind. Eng. Chem. 76 (2019) 173–180.
[9] S.J. Lee, H.H. Jo, S.K. Kwon, J.H. Lee, W.D. Kim, J.H. Lee, S.A. Park, I.K. Kwon, A novel mussel-inspired 3D printed-scaffolds immobilized with bone forming peptide-1 for bone tissue engineering applications: Preparation, characterization and evaluation of its properties, Macromol. Res. 24 (4) (2016) 305–308.
[10] D.N. Heo, N.J. Castro, S.-J. Lee, H. Noh, W. Zhu, L.G. Zhang, Enhanced bone tissue regeneration using a 3D printed microstructure incorporated with a hybrid nano hydrogel, Nanoscale 9 (16) (2017) 5055–5062.
[11] I. Gholamali, M. Yadollahi, Bio-nanocomposite polymer hydrogels containing nanoparticles for drug delivery: a review, Regener. Eng. Transl. Med. (2021) 1–18.
[12] T. Coradin, K. Wang, T. Law, L. Trichet, Type I Collagen-Fibrin Mixed Hydrogels: Preparation, Properties and Biomedical Applications, Gels 6 (4) (2020).
[13] B. Depalle, C.M. McGilvery, S. Nobakhti, N. Aldegaither, S.J. Shefelbine, A.E. Porter, Osteopontin regulates type I collagen fibril formation in bone tissue, Acta Biomater. 120 (2021) 194–202.
[14] G. Montalbano, S. Toumpaniari, A. Popov, P. Duan, J. Chen, K. Dalgarno, W. Scott III, A. Ferreira, Synthesis of bioinspired collagen/alginate/fibrin based hydrogels for soft tissue engineering, Mater. Sci. Eng. C 91 (2018) 236–246.
[15] C. Bonnans, J. Chou, Z. Werb, Remodelling the extracellular matrix in development and disease, Nat. Rev. Mol. Cell Biol. 15 (12) (2014) 786–801.
[16] H. Ragelle, A. Naba, B.L. Larson, F. Zhou, M. Prijić, C.A. Whittaker, A. Del Rosario, R. Langer, R.O. Hynes, D.G. Anderson, Comprehensive proteomic characterization of stem cell-derived extracellular matrices, Biomaterials 128 (2017) 147–159.
[17] D.N. Heo, M. Hospodiuk, I.T. Ozbolat, Synergistic interplay between human MSCs and HUVECs in 3D spheroids laden in collagen/fibrin hydrogels for bone tissue engineering, Acta Biomater. 95 (2019) 348–356.
[18] S.J. Lee, H. Nah, D.N. Heo, K.-H. Kim, J.M. Seok, M. Heo, H.-J. Moon, D. Lee, J.S. Lee, S.Y. An, Y.-S. Hwang, W.-K. Ko, S.J. Kim, S. Sohn, S.A. Park, S.-Y. Park, I.K. Kwon, Induction of osteogenic differentiation in a rat calvarial bone defect model using an In situ forming graphene oxide incorporated glycol chitosan/oxidized hyaluronic acid injectable hydrogel, Carbon 168 (2020) 264–277.
[19] M. Domingos, F. Intranuovo, A. Gloria, R. Gristina, L. Ambrosio, P. Bártolo, P. Favia, Improved osteoblast cell affinity on plasma-modified 3-D extruded PCL scaffolds, Acta Biomater. 9 (4) (2013) 5997–6005.
[20] C. Pitta Kruize, S. Panahkhahi, N.E. Putra, P. Diaz-Payno, G. Van Osch, A.A. Zadpoor, M.J. Mirzaali, Biomimetic Approaches for the Design and Fabrication of Bone-to-Soft Tissue Interfaces, ACS Biomater. Sci. Eng. (2021).
[21] J.S. Lee, H. Nah, H.-J. Moon, S.J. Lee, D.N. Heo, I.K. Kwon, Controllable delivery system: A temperature and pH-responsive injectable hydrogel from succinylated chitosan, Appl. Surf. Sci. 528 (2020) 146812.
[22] L. Buravkova, I. Larina, E. Andreeva, A. Grigoriev, Microgravity Effects on the Matrisome, Cells 10 (9) (2021) 2226.
[23] Y.R. Devaud, E. Avilla-Royo, C. Trachsel, J. Grossmann, I. Martin, M.P. Lutolf, M. Ehrbar, Label-free quantification proteomics for the identification of mesenchymal stromal cell matrisome inside 3D poly (Ethylene Glycol) hydrogels, adv. Healthcare Mater. 7 (21) (2018) 1800534.
[24] J. Jokinen, E. Dadu, P. Nykvist, J. Käpylä, D.J. White, J. Ivaska, P. Vehviläinen, H. Reunanen, H. Larjava, L. Häkkinen, J. Heino, Integrin-mediated cell adhesion to type I collagen fibrils, J. Biol. Chem. 279 (30) (2004) 31956–31963.
[25] C.-T. Hsiao, H.-W. Cheng, C.-M. Huang, H.-R. Li, M.-H. Ou, J.-R. Huang, K.-H. Khoo, H.W. Yu, Y.-Q. Chen, Y.-K. Wang, A. Chiou, J.-C. Kuo, Fibronectin in cell adhesion and migration via N-glycosylation, Oncotarget 8 (41) (2017) 70653–70668.
[26] J. Heino, The collagen family members as cell adhesion proteins, BioEssays 29 (10) (2007) 1001–1010.
[27] A.D. Theocharis, S.S. Skandalis, C. Gialeli, N.K. Karamanos, Extracellular matrix structure, Adv. Drug Deliv. Rev. 97 (2016) 4–27.
[28] J.M. Lee, S.K.Q. Suen, W.L. Ng, W.C. Ma, W.Y. Yeong, Bioprinting of Collagen: Considerations, Potentials, and Applications, Macromol. Biosci. 21 (1) (2021) 2000280.
[29] J.-Y. Exposito, U. Valcourt, C. Cluzel, C. Lethias, The fibrillar collagen family, Int. J. Mol. Sci. 11 (2) (2010) 407–426.
[30] J. Halper, M. Kjaer, Basic components of connective tissues and extracellular matrix: elastin, fibrillin, fibulins, fibrinogen, fibronectin, laminin, tenascins and thrombospondins, Progr. Heritable Soft Connective Tissue Dis. (2014) 31–47.
[31] J. Lee, G.D. Lilly, R.C. Doty, P. Podsiadlo, N.A. Kotov, In vitro toxicity testing of nanoparticles in 3D cell culture, Small 5 (10) (2009) 1213–1221.
[32] C.O. Crosby, J. Zoldan, Mimicking the physical cues of the ECM in angiogenic biomaterials, Regener. Biomater. 6 (2) (2019) 61–73.
[33] S. Buyuksungur, V. Hasirci, N. Hasirci, 3D printed hybrid bone constructs of PCL and dental pulp stem cells loaded GelMA, J. Biomed. Mater. Res. Part A (2021).
[34] R. Scaffaro, F. Lopresti, A. Maio, L. Botta, S. Rigogliuso, G. Ghersi, Electrospun PCL/GO-g-PEG structures: Processing-morphology-properties relationships, Compos. A Appl. Sci. Manuf. 92 (2017) 97–107.
[35] D. Gupta, A.K. Singh, N. Kar, A. Dravid, J. Bellare, Modelling and optimization of NaOH-etched 3-D printed PCL for enhanced cellular attachment and growth with minimal loss of mechanical strength, Mater. Sci. Eng., C 98 (2019) 602–611.
[36] H. Zhan, D.W. Löwik, A hybrid peptide amphiphile fiber PEG hydrogel matrix for 3D cell culture, Adv. Funct. Mater. 29 (16) (2019) 1808505.
[37] K. Kim, H. Thorp, S. Bou-Ghannam, D.W. Grainger, T. Okano, Stable cell adhesion affects mesenchymal stem cell sheet fabrication: effects of fetal bovine serum and human platelet lysate, J. Tissue Eng. Regener. Med. 14 (5) (2020) 741–753.
[38] J.S. Park, J.S. Chu, A.D. Tsou, R. Diop, Z. Tang, A. Wang, S. Li, The effect of matrix stiffness on the differentiation of mesenchymal stem cells in response to TGF-β, Biomaterials 32 (16) (2011) 3921–3930.
[39] Y. Kim, J.Y. Lim, G.H. Yang, J.-H. Seo, H.-S. Ryu, G. Kim, 3D-printed PCL/bioglass (BGS-7) composite scaffolds with high toughness and cell-responses for bone tissue regeneration, J. Ind. Eng. Chem. 79 (2019) 163–171.
[40] W.-K. Ko, D.N. Heo, H.-J. Moon, S.J. Lee, M.S. Bae, J.B. Lee, I.-C. Sun, H.B. Jeon, H. K. Park, I.K. Kwon, The effect of gold nanoparticle size on osteogenic differentiation of adipose-derived stem cells, J. Colloid Interface Sci. 438 (2015) 68–76.
[41] H. Nah, D. Lee, M. Heo, J.S. Lee, S.J. Lee, D.N. Heo, J. Seong, H.-N. Lim, Y.-H. Lee, H.-J. Moon, Y.-S. Hwang, I.K. Kwon, Vitamin D-conjugated gold nanoparticles as functional carriers to enhancing osteogenic differentiation, Sci. Technol. Adv. Mater. 20 (1) (2019) 826–836.
[42] J.A. Gordon, C.E. Tye, A.V. Sampaio, T.M. Underhill, G.K. Hunter, H.A. Goldberg, Bone sialoprotein expression enhances osteoblast differentiation and matrix mineralization in vitro, Bone 41 (3) (2007) 462–473.
[43] H.-S. Kim, M. Kim, D. Kim, E.-J. Choi, S.H. Do, G. Kim, 3D macroporous biocomposites with a microfibrous topographical cue enhance new bone formation through activation of the MAPK signaling pathways, J. Ind. Eng. Chem. 104 (2021) 478–490.

[44] M.N. Collins, G. Ren, K. Young, S. Pina, R.L. Reis, J.M. Oliveira, Scaffold Fabrication Technologies and Structure/Function Properties in Bone Tissue Engineering, Adv. Funct. Mater. 31 (21) (2021) 2010609.
[45] S.J. Lee, J.E. Won, C. Han, X.Y. Yin, H.K. Kim, H. Nah, I.K. Kwon, B.H. Min, C.H. Kim, Y.S. Shin, S.A. Park, Development of a three-dimensionally printed scaffold grafted with bone forming peptide-1 for enhanced bone regeneration with in vitro and in vivo evaluations, J Colloid Interface Sci 539 (2019) 468–480.
[46] S.J. Lee, M.S. Bae, D.W. Lee, D.N. Heo, D. Lee, M. Heo, S.J. Hong, J. Kim, W.D. Kim, S.A. Park, I.K. Kwon, The use of heparin chemistry to improve dental osteogenesis associated with implants, Carbohyd Polym 157 (2017) 1750–1758.
[47] S. Yin, W. Zhang, Z. Zhang, X. Jiang, Recent Advances in Scaffold Design and Material for Vascularized Tissue-Engineered Bone Regeneration, Adv Healthc Mater 8 (10) (2019) 1801433.
[48] F. Pati, T.-H. Song, G. Rijal, J. Jang, S.W. Kim, D.-W. Cho, Ornamenting 3D printed scaffolds with cell-laid extracellular matrix for bone tissue regeneration, Biomaterials 37 (2015) 230–241.